Structural and electronic properties of superconducting Heusler alloy $Ni_2Nb_{1+x}Sn_{1-x}$: *Ab-initio* approach

Soumyadipta Pal [a,b]

[a] *Satyendra Nath Bose National Centre for Basic Sciences[Department of Science & Technology, Government of India], Block-JD, Sector-III, Salt Lake, Kolkata 700098, India. Phone: +91 (033) 2335 5706-8 Fax : +91 (033) 2335 3477.*

[b] *soumyadipta.pal@gmail.com*

Abstract

Using *ab initio* calculation, we investigate systematically the structural and electronic properties of $Ni_2Nb_{1+x}Sn_{1-x}$ (x = 0, 0.25, 0.50). Here, projector augmented wave approach (PAW) implemented in the Vienna ab initio simulation package (VASP) within generalized gradient approximation (GGA) for the exchange-correlation functional has been used. In this article, it is reported that though Ni_2NbSn and $Ni_2Nb_{1.25}Sn_{0.75}$ have no structural transformation, $Ni_2Nb_{1.5}Sn_{0.5}$ can transform to tetragonal structure from cubic $L2_1$ phase. The cubic lattice parameter decreases with Nb doping at Sn sites in off-stoichiometric alloys. The alloys are in paramagnetic phase in all the structures. The hybridization between Ni and Nb 3d states triggers the tetragonal distortion. Due to Nb doping in cubic $L2_1$ phase, there is a significant change in total density of states (DOS) at Fermi energy (E_F) ($N(E_F)$). $N(E_F)$ increases with increasing Nb doping. But, $N(E_F)$ decreases during structural transformation of $Ni_2Nb_{1.5}Sn_{0.5}$. The superconducting critical temperature (T_C) also changes with Nb doping in cubic phase and tetragonal distortion because T_C very much depends on $N(E_F)$.

1 INTRODUCTION

Heusler alloys are ternary intermetallic compounds which can be defined by stoichiometric formula X_2YZ, where X and Y are transition elements and Z is a III, IV, or V group element [1]. Cu_2MnSn was the first Heusler alloy discovered by F. Heusler in 1903 [2]. Subsequently, a large number of Heusler alloys have been discovered with a wide range of physical properties. These class of materials present different magnetic properties like itinerant and localized magnetism, antiferromagnetism, helimagnetism, Pauli paramagnetism or heavy-fermionic behavior [3, 4, 5, 6, 7, 8, 9, 10, 11, 12, 13, 14]. Along with magnetic diversity, the alloys have acquired recent interest depending on electrical transport properties [6], shape memory effect [15], half-metallic ferromagnetism [16], and semimetallic [8, 9] behavior. Moreover, several Heusler compounds with 27 valence electrons have been discovered to have a superconducting ground state [17, 18, 19, 20, 21, 22, 23]. Recently, T. Klimczuk *et al.* has listed wide varity of superconducting Heusler alloys [24].

One of the superconducting Heusler alloys is Ni_2NbSn. This is crystalized in cubic $L2_1$ phase [23] in room temperature which is same as the other Ni based Heusler alloys [25]. Previously, some research groups [23, 26, 27] have mentioned the superconductivity, specific heat and electrical properties of Ni_2NbSn. Among all the reported Ni based superconducting Heusler alloys [24], this stoichiometric alloy has highest T_C of 3.4 K [24, 27]. Unfortunately, there is no reported data available about the properties of off-stoichiometric $Ni_2Nb_{1+x}Sn_{1-x}$ alloys. So, the alloys have a lot of research scope in experimental as well as theoretical point of view. The aim of the present paper is to understand the structural and electronic properties of Ni_2NbSn and its off-stoichimetric alloys theoretically. There are some fundamental questions, whether Ni-Nb-Sn alloys have structural and magnetic transitions and how the T_C varies in off-stoichiometric alloys. So, here the theoretical *ab-initio* calculation is adopted to find out the change in structural and magnetic properties as well as the variation of DOS of atomic orbitals with Nb doping at Sn sites of off-stoichiometric alloys, because change of value of the DOS at E_F changes the T_C appreciably.

2 COMPUTIONAL DETAILS

In the last two decades, tremendous progress in the development of methods for *ab initio* calculations have been witnessed to understand electronic structure and material properties. This development was based on density-functional theory (DFT), which considers the complexity of the electron-electron interactions in many-electron systems into an effective one-electron potential, which is a functional of electron density only [28, 29].

One of the most accurate calculation can be done by VASP, developed by Georg Kresse and his coworkers [30, 31]. In this paper, the electronic structure of Ni-Nb-Sn alloys have been investigayed by the VASP. VASP is a plane-wave code for ab-initio density-functional calculations. It tries to match the accuracy of the most advanced all electron codes by using PAW approach [32, 33] for describing the electron-ion interaction. Furthermore, the electronic exchange and correlation energies are described by using the GGA of Perdew *et al.* [34, 35]. In VASP, pseudopotentials have been introduced to avoid the need for an explicit treatment of the strongly bound and chemically inert core electrons.

For electronic structure calculation of Ni_2NbSn, cubic $L2_1$ structure having $Fm\bar{3}m$ space group with atomic positions 8*c* (Ni), 4*b* (Nb) and 4*a* (Sn) is used. Starting with the experimental lattice parameter $a = 6.157\mathring{A}$ [23] of 16 atom unit cell, convergence test of KPOINTS and ENCUT has been

performed considering ground state energy difference (ΔE0) $\sim$ 5 meV. The optimized plane wave cut off energy (ENCUT) of 450 eV and Monkhorst-Pack KPOINTS grid of 12×12×12 are employed for the calculation. Next, the lattice parameter (a) is relaxed so as to minimize the total ground state energy (E0)/unit cell. Afterward, Nb is doped at Sn sites in off-stoichiometric $Ni_2Nb_{1+x}Sn_{1-x}$ according to $x = 0.25$ and 0.5. The lattice parameters of the off-stoichiometric alloys are also relaxed to minimize E0/unit cell. Using the equilibrium structure, spin integrated total DOS per unit cell and partial density of states (PDOS) per atom are calculated. The input cubic $L2_1$ crystal structures of $Ni_2Nb_{1+x}Sn_{1-x}$ for $x = 0$, 0.25 and 0.5 are shown in Fig. 1. Here Nb1 and Nb2 indicate the Nb atoms which are situated at the parent Nb sites and at the Sn sites respectively.

In Fig. 1, the particular doping combination of Nb at Sn sites of $Ni_2Nb_{1.25}Sn_{0.75}$ and $Ni_2Nb_{1.5}Sn_{0.5}$ are equivalent to other possible combinations. Results remain unchanged for all possible configurations. So, the present doping combinations are reliable to use for calculations.

3 RESULTS AND DISCUSSIONS

3.1 Structural and magnetic properties

First, we shall concentrate on the cubic structure of $Ni_2Nb_{1+x}Sn_{1-x}$. In Fig. 2, ground state energy E0 (eV)/unit cell of Ni_2NbSn, $Ni_2Nb_{1.25}Sn_{0.75}$ and $Ni_2Nb_{1.5}Sn_{0.5}$ with respect to volume of cubic $L2_1$ structure are plotted. The theoretical E0/unit cell vs. volume curve is fitted with Murnaghan equation of state [36, 37, 38, 39]. It is observed that the equilibrium volume as well as the theoretical lattice parameter of $Ni_2Nb_{1+x}Sn_{1-x}$ decrease with doped Nb concentration (x).

The equilibrium unit cell volume and theoretical lattice parameters of $Ni_2Nb_{1+x}Sn_{1-x}$ for $x = 0$, 0.25 and 0.5 are listed in the Table 1.

From Table 1, it is observed that the equilibrium lattice parameter of unit cell of Ni_2NbSn is in good agreement with experimental value [23] within 1 %. Unfortunately, there is no experimental data available for lattice parameters of off-stoichiometric Ni-Nb-Sn alloys. It is obtained that, the theoretical lattice parameter of unit cell of $Ni_2Nb_{1+x}Sn_{1-x}$ decreases with increasing concentration of Nb doping at Sn sites. Due to smaller size of Nb than Sn, the unit cell volume of off-stoichiometric alloys become less than the stoichiometric one. The change of theoretical lattice parameters with doped Nb concentration is depicted in Fig. 3. It is observed that the lattice parameter decreases linearly. So, from the trend of variation of theoretical lattice parameters, cubic unit cell lattice parameters of unknown compositions can be obtained.

In the E0/unit cell vs. volume calculation, only the ionic positions of unit cell were relaxed for different cubic unit cell lattice parameters of $Ni_2Nb_{1+x}Sn_{1-x}$. Now, to find out whether Ni-Nb-Sn alloys have any structural transition, the ionic positions and volume of unit cells of $Ni_2Nb_{1+x}Sn_{1-x}$ ($x = 0$, 0.25, 0.5) are relaxed. Interestingly, it is obtained that Ni_2NbSn and $Ni_2Nb_{1.25}Sn_{0.75}$ have no structural transformation. But, $Ni_2Nb_{1.5}Sn_{0.5}$ transforms to tetragonal structure where one axis elongates along one direction and the other two axes contract along the other two directions. For example, here a elongates and b & c contract. The equilibrium tetragonal structure of $Ni_2Nb_{1.5}Sn_{0.5}$ is of lattice parameters $a = 7.31\mathring{A}$, $b = 5.70\mathring{A}$ and $c = 5.70\mathring{A}$. Due to formation of Nb cluster in bc plane the b and c axes contract and due to strong interaction between Ni & Nb a axis elongates. By this distortion, the system lowers its energy. In Table 2, the nearest neighbor distances between Ni & Nb1 and Ni & Nb2 of $Ni_2Nb_{1.5}Sn_{0.5}$ are listed in both cubic and tetragonal structures.

From the Table 2, it is observed that there are two different Ni-Nb1 distances. The distance 2.64 $\AA$ of Ni-Nb1 bond of cubic structure increases to 2.71 $\AA$ due to tetragonal transformation. This Nb1 is situated in the Nb1-Sn plane (see Fig. 1). The distance 2.73 $\AA$ of Ni-Nb1 and Ni-Nb2 does not change due to structural transformation. These Nb1 and Nb2 are placed in the plane of Nb cluster. The tetragonal distortion of $Ni_2Nb_{1.5}Sn_{0.5}$ is quite similar to the ferromagnetic $Ni_2Mn_{1.5}Sn_{0.5}$ [40]. Here, Ni-Mn (at Sn sites) hybridization prompts the structural distortion. So, from the analogy, it is argued that hybridization between Ni and Nb (at Sn sites) states helps in tetragonal distortion of cubic $L2_1$ structure.

In the following subsection, the total DOS and PDOS of Ni-Nb-Sn alloys in both cubic and tetragonal phases will be discussed to understand how atomic orbitals behave due to the Nb doping at Sn sites in cubic structure and structural transformation of $Ni_2Nb_{1.5}Sn_{0.5}$.

Though $Ni_2Nb_{1+x}Sn_{1-x}$ for $x = 0$, 0.25 and 0.5 have such structural varieties, there are no magnetic transitions of these alloys. All the alloys are in paramagnetic ground state. So, magnetic moments are very less. This is contrast to the Ni based Heusler alloys. As elementary Ni is ferromagnetic in nature, Ni-containing Heusler compounds with high proportion of Ni are definitely expected to show magnetic order [41]. But, here the presence of Nb states disrupts the magnetic order of Ni states giving rise to paramagnetism of these systems. Some research groups [23, 27, 42] have also mentioned the paramagnetic contribution to the magnetic susceptibility of Ni_2NbSn. Waki *et al.* [23] identified experimentally that the magnetic susceptibility of these compounds shows temperature independent Pauli paramagnetism. According to them, the small amounts of magnetic susceptibility are consistent with the small values of DOS which is derived from specific heat measurements. From the values of DOS and temperature independent susceptibility, it is considered that the Fermi level is situated near a minimum in the DOS. Regrettably, there is no experimental data of paramagnetic susceptibility of off-stoichiometric Ni-Nb-Sn alloys in the literature.

3.2 Density of states in cubic and tetragonal phase

In Fig. 4, 5, 6, 7 and 8, the spin integrated total DOS, PDOS of Ni, Nb1, Nb2 and Sn of $Ni_2Nb_{1+x}Sn_{1-x}$ ($x = 0$, 0.25 and 0.5) in cubic $L2_1$ structure are depicted respectively.

From Fig. 4, it is obtained that the valence band width of total DOS is 11 eV. From the PDOS plots of different atoms, it is obvious that the contributions to total DOS from 4 eV to -3 eV are mainly due to Ni, Nb1 and Nb2 t_{2g} and e_g states; but Ni s and Nb1 and Nb2 s and p states are much smaller. From Fig. 6 and 7, it is observed that around E_F, above and below the Fermi surface the contribution to the total DOS is mainly due to Nb1 and Nb2 3d states. According to J. Winterlink *et al.* [43], a saddle point at a certain high-symmetry point in the energy dispersion curve at E_F leads to a high DOS at E_F. These are referred to as Van Hove singularities (VHS) [44]. Superconducting Heusler compounds with 27 electrons exhibit saddle point close to E_F in the corresponding energy dispersion curve according to the van Hove scenario [45, 41, 46]. Here, the VHS are situated around 1 eV just above E_F. Those singularities are mainly contributed by Nb 3d states. This same situation arises in other superconducting Heusler alloys [42, 43, 41, 46]. Furthermore, near E_F around -0.4 eV there exists a minima in DOS. In 1985, Waki *et al.* [23] predicted the same situation experimentally, which is consistent with paramagnetism of the system. From Fig. 3 and 5, it is observed that arond -1 eV energy, the states are mainly Ni e_g states. In the energy range -1.7 to -3.1 eV, the states are contributed by Ni e_g and t_{2g}, Nb1 t_{2g} and Nb2 e_g & t_{2g}. Due to tetrahedron field of Nb atoms, degeneracy of Ni 3d orbitals splits into up-lying twofold e_g states and low-lying threefold t_{2g} states.

From Fig. 4, 5, 6 and 7, it is obtained that the states around -4 eV are composed of Ni and Nb s states. From Fig. 4 and 8, it is observed that the states around -6 eV and -10 eV, are contributed by Sn p and s states respectively. Moreover, the gap in the energy range -6.9 to -8.5 eV is the typical behavior of Heusler alloys [46].

Now, in this context to see the effect of Nb doping at Sn sites in the cubic structure of off-stoichiometric $Ni_2Nb_{1+x}Sn_{1-x}$, we shall concentrate on total DOS at and around E_F for $x = 0$, 0.25 and 0.5. The values of $N(E_F)$ with x concentration are listed in Table 3. From inset of Fig. 3 and Table 3, it is clearly seen that $N(E_F)$ increases with Nb doping. This occurs because at E_F, the total DOS is mainly contributed by Nb 3d states and Nb PDOS increases with Nb doping. The value of DOS at E_F is significant because the value of T_C is dependent on $N(E_F)$. According to BCS theory [47], $T_C = 1.13\Theta_D \exp\left[-\frac{1}{UN(E_F)}\right]$; where Θ_D is the Debye temperature and U is the electron-electron attractive interaction which is constant for the present alloys. Debye temperature can be written as, $\Theta_D = \frac{\hbar v}{k_B}\left(\frac{6\pi^2 N}{V}\right)^{\frac{1}{3}}$ [48]. In this defination, if N is the number of primitive cells in any specimen of volume V, the total no. of acoustic phonon modes is N. In the Ni-Nb-Sn 16 atom unit cell, there is only one primitive cell inside. So, $\Theta_D = \frac{\hbar v}{k_B}\left(\frac{6\pi^2}{V_0}\right)^{\frac{1}{3}}$, where V_0 is the volume of the unit cell and v is the velocity of sound in the alloy which is constant for Ni-Nb-Sn alloys. From Table 1, it has been observed that V_0 decreases in off-stoichiometric alloys due to doping of Nb. As a result, Θ_D increases. So, owing to increase of both Θ_D and $N(E_F)$, the T_C increases in off-stoichiometric Ni-Nb-Sn alloys.

Moreover, the VHS shift towards the higher energy side from E_F and the maxima of DOS decreases with increasing x concentration. Due to Nb doping, number of valence electrons increases in the system. So, doping with charge carriers does not only change the density in the system but also smears the density of states diminishing the singularities [49].

In Fig. 9 and 10, spin integrated total DOS and Ni, Nb1 and Nb2 e_g and t_{2g} PDOS of $Ni_2Nb_{1.5}Sn_{0.5}$ in cubic $L2_1$ and tetragonal structures are depicted respectively. To understand the effect of tetragonal distortion on DOS, here we shall concentrate on DOS around E_F.

From inset of Fig. 9, it is observed that the $N(E_F)$ decreases due to tetragonal distortion. This happens due to the Nb 3d DOS at E_F decreases in tetragonal structure (see Fig. 10). The values of $N(E_F)$ of $Ni_2Nb_{1.5}Sn_{0.5}$ in cubic $L2_1$ and tetragonal structures are listed in Table 4.

Due to tetragonal transformation, the volume of the cubic unit cell remains almost unchanged. So, the Debye temperature becomes constant in both cubic and tetragonal unit cell structures. Finally, due to decrease of $N(E_F)$ from cubic to tetragonal phase, T_C decreases.

From Fig. 9, it is also observed that, the Ni e_g peak at -0.94 eV shifts to -0.44 eV due to tetragonal distortion from cubic phase. This happens owing to hybridization between Ni and Nb e_g states. Moreover, it is observed that the VHS disappear due to tetragonal distortion. This happens because some occupied Ni e_g states shifts towards higher energy side after structural distortion and become unoccupied. Increasing DOS above E_F causes the disappearance of VHS and the system becomes stable.

4 CONCLUSIONS

In summary, we would like to emphasize the important results of this article more precisely. Firstly, the theoretical cubic unit cell lattice parameter of Ni_2NbSn is in well agreement with experimental value

[23] within 1 %. So, the theoretical lattice parameter values of off-stoichiometric $Ni_2Nb_{1+x}Sn_{1-x}$ is expected to be also good agreement with the experiment. Second important point is that due to increasing concentration of Nb doping at Sn sites the theoretical cubic lattice parameters of off-stoichiometric alloys decrease. Due to smaller size of Nb than Sn, the unit cell volume of off-stoichiometric alloys become less than the stoichiometric Ni_2NbSn. The trend of decrease of lattice parameters is linear in nature. So, from this tendency of linear behavior of lattice parameters, cubic unit cell lattice parameters of unknown compositions can be obtained. Next valuable result is that Ni_2NbSn and $Ni_2Nb_{1.25}Sn_{0.75}$ have no structural transformation if the cubic structure is allowed to be fully relaxed. Interestingly, $Ni_2Nb_{1.5}Sn_{0.5}$ transforms to tetragonal structure where one axis elongates along one direction and the other two axes contract along the other two directions. Furthermore, it is observed that there is no magnetic phase transition along with structural transformation of Ni-Nb-Sn alloys. All the alloys are in paramagnetic ground state. The presence of Nb atom interrupts the ferromagnetic order of Ni atom. This gives rise to paramagnetism of the system. These results are very important because till now no experimental and theoretical information of structural and magnetic properties of off-stoichiometric $Ni_2Nb_{1+x}Sn_{1-x}$ have been discussed in literature. Moreover, density of states plots of $Ni_2Nb_{1+x}Sn_{1-x}$ for $x = 0$, 0.25 and 0.50 give the idea how the electronic structure changes with Nb doping. First interesting result is obtained that VHS just above E_F, shift towards the higher energy side from E_F and the maximum value of DOS decreases with increasing Nb doping concentration. The VHS are mainly contributed by Nb 3d states. Doping with Nb increases the number of valence electrons in the system and increasing number of charge carriers smears the DOS out of Fermi sphere eliminating the singularities. It is also obtained that $N(E_F)$ increases with increasing concentration of doped Nb. This happens because at E_F, the total DOS is contributed by Nb 3d states and Nb PDOS increases with Nb doping. Now, T_C very much depends on $N(E_F)$. BCS theory [47] predicted, $T_C = 1.13\Theta_D \exp\left[-\frac{1}{UN(E_F)}\right]$. Due to increase of both Θ_D and $N(E_F)$ with increasing concentration of Nb doping, T_C increases in off-stoichiometric Ni-Nb-Sn alloys. This result is also completely new and increasing T_C has a great interest in making high temperature superconducting materials. Furthermore, due to tetragonal distortion of $Ni_2Nb_{1.5}Sn_{0.5}$, $N(E_F)$ decreases as Nb 3d PDOS decreases. In this context, one important point should be mentioned that hybridization between Ni and Nb 3d states triggers the tetragonal distortion of $Ni_2Nb_{1.5}Sn_{0.5}$. Due to tetragonal transformation, the volume of the cubic unit cell remains almost unaltered. So, the Debye temperature becomes constant in both cubic and tetragonal unit cell structures. Finally, due to decrease of $N(E_F)$ from cubic to tetragonal phase, T_C decreases. Moreover, the VHS disappear due to tetragonal distortion. This occurs because some occupied Ni e_g states shifts towards higher energy side after tetragonal distortion and become unoccupied. Increasing DOS above E_F causes the diminish of VHS. Due to this mechanism, the distorted structure becomes stable of $Ni_2Nb_{1.5}Sn_{0.5}$. Thus, this paper gives a deep insight of structural and electronic properties of superconducting $Ni_2Nb_{1+x}Sn_{1-x}$ Heusler alloy.

5 ACKNOWLEDGMENTS

The Author would like to thank Satyendra Nath Bose National Centre for Basic Sciences[Department of Science & Technology, Government of India], for financial help.

References

[1] H. Rached, D. Rached, R. Khenata, Ali H. Reshak, and M. Rabah, Phys. Status Solidi B 246, 1580 (2009).

[2] F. Heusler, Verh. Dtsch. Phys. Ges. 5, 219 (1903).

[3] P. J. Webster, and K. R. A. Ziebeck, Alloys and Compounds of d-Elements with Main Group Elements. Part 2., Landolt-Bornstein, New Series, Group III, vol 19c, ed. by H. R. J. Wijn, (Springer, Berlin 1988) pp 75-184.

[4] K. R. A. Ziebeck, and K. U. Neumann, Magnetic Properties of Metals, ed. by H. R. J. Wijn, Landolt-Boörnstein, New Series, Group III, vol 32/c(Springer, Berlin 2001) pp 64-414.

[5] P. J.Webster, and K. R. A. Ziebeck, J. Phys. Chem. Solids 34, 1647 (1973).

[6] J. Pierre, R. V. Skolozdra, J. Tobola, C. Hordequin, M. A. Kouacou, I. Karla, R. Currat, and E. Lelièvere-Berna, J. Alloys Compd. 262-263, 101 (1997).

[7] J. Tobola and J. Pierre, J. Alloys Compd. 296, 243 (2000).

[8] D. Kaczorowski, K. Gofryk, T. Plackowski, A. Leithe-Jasper, and Yu. Grin, J. Magn. Magn. Mater. 290-291, 573 (2005).

[9] K. Gofryk, D. Kaczorowski, T. Plackowski, A. Leithe-Jasper, and Y. Grin, Phys. Rev. B 72, 094409 (2005).

[10] S. Takayanagi, S. B. Woods, N. Wada, T. Watanabe, Y. $\overline{O}$nuki, A. Kobori, T. Komatsubara,M. Imai, and H. Asano, J. Magn. Magn. Mater. 76-77, 281 (1988).

[11] H. Nakamura, Y. Kitaoka, K. Asayama, Y. $\overline{O}$nuki, and T. Komatsubara, J. Magn. Magn. Mater. 76-77, 467 (1988).

[12] R. Lahiouel, J. Pierre, E. Siaud, R. M. Galera, M. J. Besnus, J. P. Kappler, and A. P. Murani, Z. Phys. B 67, 185 (1987).

[13] D. Kaczorowski, A. Leithe-Jasper, T. Cichorek, K. Tenya, J. Custers, P. Gegenwart, and Yu. Grin, Acta Phys. Pol. B 34, 1253 (2003).

[14] K. Gofryk, D. Kaczorowski, and A. Czopnik, Solid State Commun. 133, 625 (2005).

[15] Z. H. Liu, M. Zhang, Y. T. Cui, Y. Q. Zhou,W. H.Wang, G. H.Wu, X. X. Zhang, and Gang Xiao, Appl. Phys. Lett. 82, 424 (2003), and references therein.

[16] Z. Yao, S. Gong, J. Fu, Y. -S. Zhang, and K. -L. Yao, Solid State Commun. 150, 2239 (2010), and references therein.

[17] M. Ishikawa, J. L. Jorda, and A. Junod, Superconductivity in d- and f-Band Metals (Kernforschungszentrum, Karlsuhe, 1982), p. 141.

[18] M. J. Johnson, and R. N. Shelton, Solid State Commun. 52, 839 (1984).

[19] R. N. Shelton, L. S. Hausermann-Berg, M. J. Johnson, P. Klavins, and H. D. Yang, Phys. Rev. B 34, 199 (1986).

[20] H. A. Kierstead, B. D. Dunlap, S. K. Malik, A. M. Umarji, and G. K. Shenoy, Phys. Rev. B 32, 135 (1985).

[21] C. L. Seaman, N. R. Dilley, M. C. de Andrade, J. Herrmann, M. B. Maple, and Z. Fisk, Phys. Rev. B 53, 2651 (1996).

[22] J. H. Wernick, G.W. Hull, T. H. Geballe, J. E. Bernardini, and J. V. Waszczak, Mater. Lett. 2, 90 (1983).

[23] S. Waki, Y. Yamaguchi, and K. Mitsugi, J. Phys. Soc. Jpn. 54, 1673 (1985).

[24] T. Klimczuk, C. H. Wang, K. Gofryk, F. Ronning, J. Winterlik, G. H. Fecher, J. C. Griveau, E. Colineau, C. Felser, J. D. Thompson, D. J. Safarik, and R. J. Cava, Phys. Rev. B 85, 174505 (2012).

[25] Y. Sutou, Y. Imano, N. Koeda, T. Omori, R. Kainuma, K. Ishida and K. Oikawa, Appl. Phys. Lett. 85, 4358 (2004).

[26] M.A.S. Boff, G.L.F. Fraga, D.E. Brandão, and A.A. Gomes, J. Magn. Magn. Mater 153, 135 (1996).

[27] J. H. Wernick, G. W. Hull, T. H. Geballe, J. E. Bernardini, and J. V. Waszczak, Materials Letters 2, 90 (1983).

[28] T. Kanomata, K. Fukushima, H. Nishihara, R. Kainuma, W. Ito, K. Oikawa, K. Ishida , K. -U. Neumann, and K.R.A. Ziebeck, Mater. Sci. Forum 583, 119 (2008).

[29] J. Hafner, Ab-Initio Simulations of Materials Using VASP: Density-Functional Theory and Beyond, Wiley InterScience (2008).

[30] G. Kresse, and J. Hafner, Phys. Rev. B 47, 558 (1993).

[31] G. Kresse, and J. Furthmüller, Comput. Mater. Sci. 6, 15 (1996); Phys. Rev. B 54, 11169 (1996).

[32] P. E. Blöchl, Phys. Rev. B 50, 17953 (1994).

[33] G. Kresse, and D. Joubert, Phys. Rev. B 59, 1758 (1999).

[34] J. P. Perdew, J. A. Chevary, S. H. Vosko, K. A. Jackson, M. R. Pederson, D. J. Singh, and C. Fiolhais, Phys. Rev. B 46, 6671 (1992).

[35] J. P. Perdew, K. Burke, and M. Ernzerhof, Phys. Rev. Lett. 77, 3865 (1996).

[36] F. Murnaghan, Proc. Nat. Acad. Sci. USA 30, 244 (1944).

[37] F.D. Murnaghan, Finite Deformation of an Elastic Solid, Dover, New York, 1995.

[38] J. Poirier, Introduction to the Physics of the Earth's Interior, Cambridge University Press, Cambridge, 1991.

[39] V.G. Tyuterev, and N. Vast, Computational Materials Science 38, 350 (2006).

[40] M. Ye, A. Kimura, Y. Miura, M. Shirai, Y. T. Cui, K. Shimada, H. Namatame, M. Taniguchi, S. Ueda, K. Kobayashi, R. Kainuma, T. Shishido, K. Fukushima, and T. Kanomata, Phys. Rev. Lett. 104, 176401 (2010).

[41] J. Winterlik, G. H. Fecher, A. Thomas, C. Felser, M. Jourdan, K. Grube, F. Hardy, H. V. Löhneysen, K. L. Holman, and R. J. Cava, Phys. Rev. B 78, 184506 (2008).

[42] W. Ming, Y. Liu, W. Zhang, J. Zhao, and Y. Yao, J. Phys.: Condens. Matter 21, 075501 (2009).

[43] J. Winterlik, G. H. Fecher, A. Thomas, and C. Felser, Phys. Rev. B 79, 064508 (2009).

[44] L. V. Hove, Phys. Rev. 89, 1189 (1953).

[45] C. Felser, J. Solid State Chem. 160, 93 (2001).

[46] J. Winterlik, G. Fecher, and C. Felser, Solid State Commun. 145, 475 (2008).

[47] J. Bardeen, L. N. Cooper, and J. R. Schrieffer, Phys. Rev. 108, 1175 (1957).

[48] Charles Kittel, Introduction To Solid State Physics, John Wiley & Sons, Inc., New York, 7th Ed., 2007.

[49] G. Litak, Phys. Stat. Sol. (b) 229, 1427 (2002).

6 Tables

Table 1: List of equilibrium unit cell volume, theoretical lattice parameters of $Ni_2Nb_{1+x}Sn_{1-x}$ for x = 0, 0.25 and 0.5 in cubic $L2_1$ phase and experimental lattice parameter of Ni_2NbSn.

Doped Nb concentration (x)	Equilibrium unit cell volume ($\AA^3$)	Equilibrium theoretical lattice parameter ($\AA$)	Experimental lattice parameter ($\AA$)
0.00	239.938	6.214	6.157 [23]
0.25	239.030	6.206	-
0.50	238.201	6.199	-

Table 2: Nearest neighbor distances between Ni & Nb1 and Ni & Nb2 of $Ni_2Nb_{1.5}Sn_{0.5}$ in both cubic $L2_1$ and tetragonal structures.

Structure	Ni-Nb1 ($\AA$)	Ni-Nb2 ($\AA$)
Cubic	2.64, 2.73	2.73
Tetragonal	2.71, 2.73	2.73

Table 3: List of theoretical values of $N(E_F)$ of $Ni_2Nb_{1+x}Sn_{1-x}$ for x = 0, 0.25 and 0.5 in cubic $L2_1$ phase.

Doped Nb concentration (x)	$N(E_F)$ (states/eV cell)
0.00	10.34
0.25	17.31
0.50	18.43

Table 4: List of theoretical values of $N(E_F)$ of $Ni_2Nb_{1.5}Sn_{0.5}$ in cubic $L2_1$ and tetragonal phase.

Crystal structure	$N(E_F)$ (states/eV cell)
Cubic	18.51
Tetragonal	14.99

7 Figures

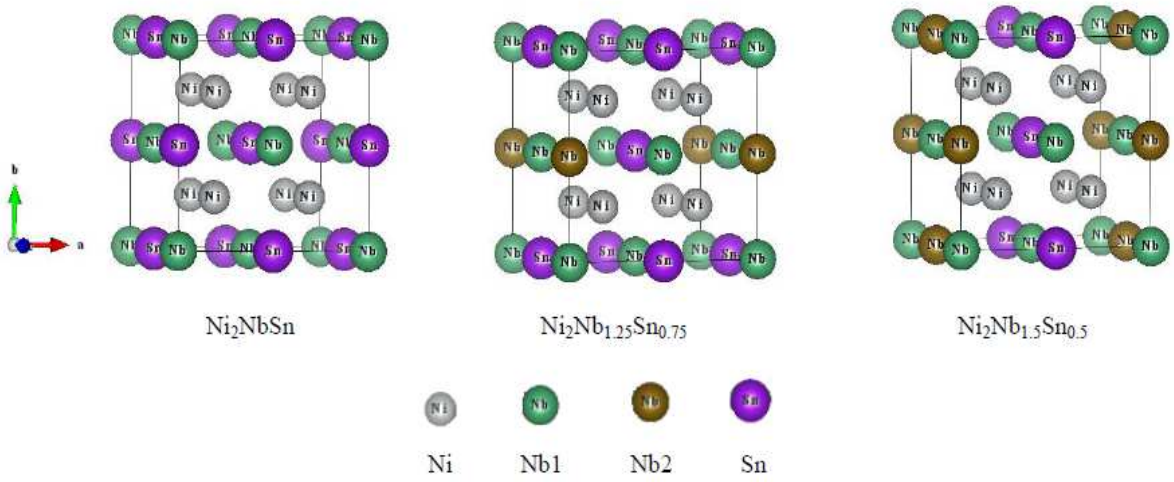

Figure 1: Cubic $L2_1$ structures of $Ni_2Nb_{1+x}Sn_{1-x}$ for $x = 0$, 0.25 and 0.5.

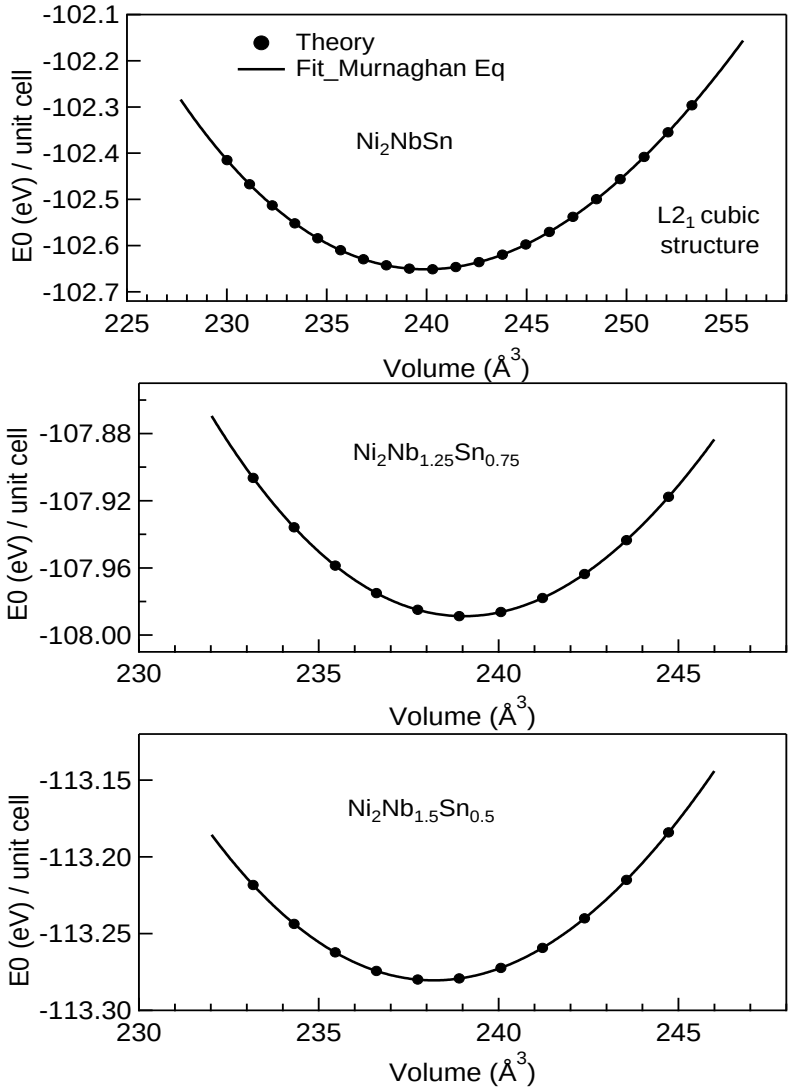

Figure 2: Total ground state energy (E0)/ unit cell and fitted curve vs. volume plot of $Ni_2Nb_{1+x}Sn_{1-x}$ for $x = 0$, 0.25 and 0.5 in cubic $L2_1$ structure.

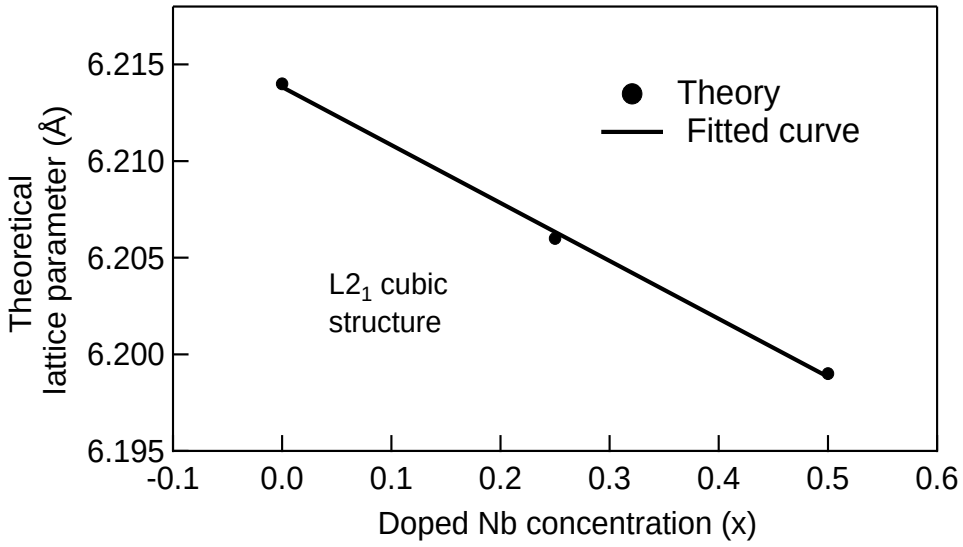

Figure 3: Theoretical lattice parameter and fitted curve vs. doped Nb concentration (x) plot of $Ni_2Nb_{1+x}Sn_{1-x}$ for $x = 0$, 0.25 and 0.5 in cubic $L2_1$ structure.

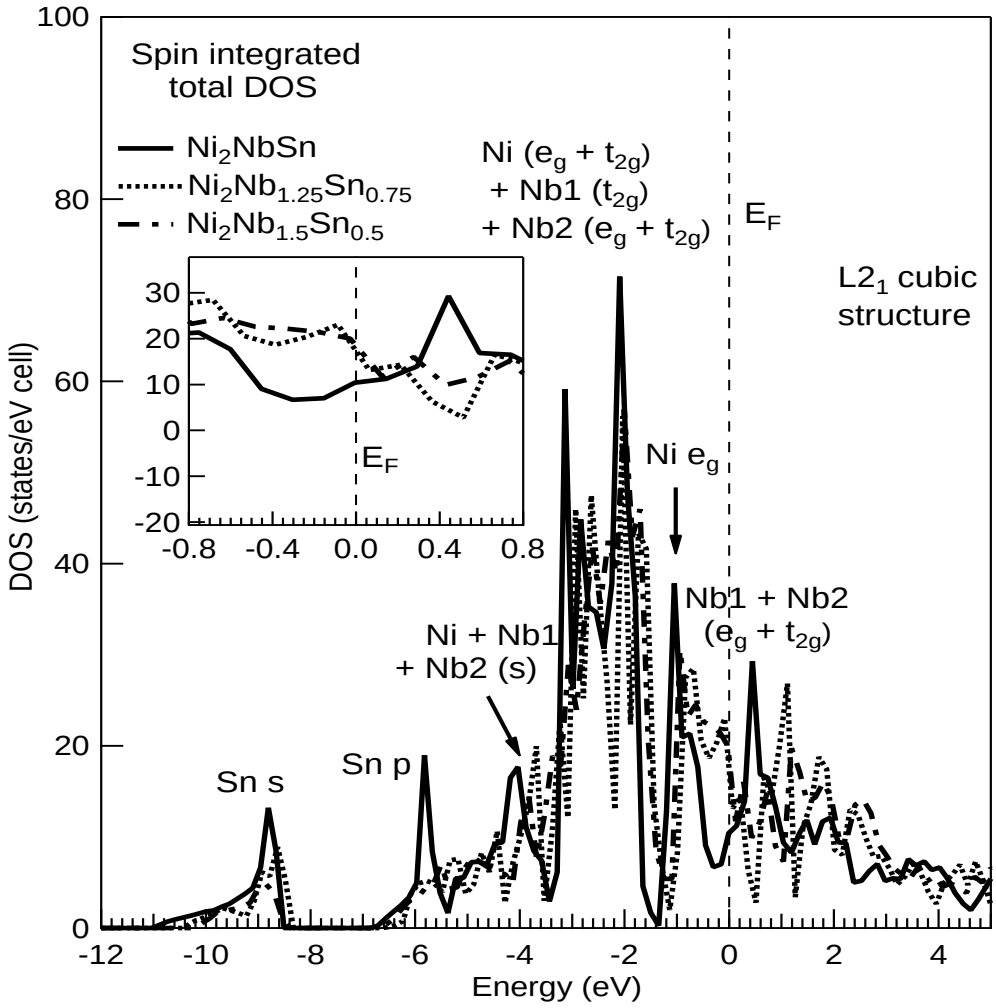

Figure 4: Spin integrated total DOS plot of $Ni_2Nb_{1+x}Sn_{1-x}$ for $x = 0$, 0.25 and 0.5 in cubic $L2_1$ structure.

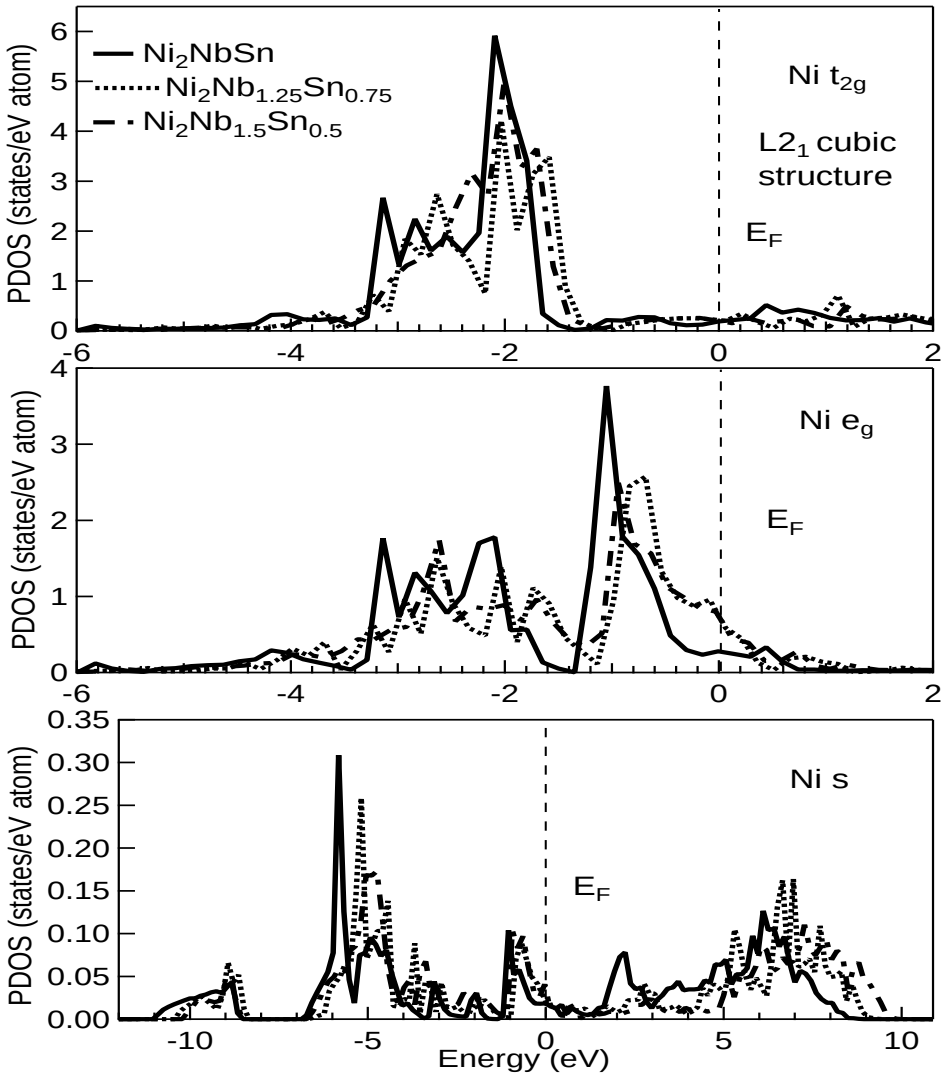

Figure 5: Spin integrated Ni PDOS of $Ni_2Nb_{1+x}Sn_{1-x}$ for $x = 0$, 0.25 and 0.5 in cubic $L2_1$ structure.

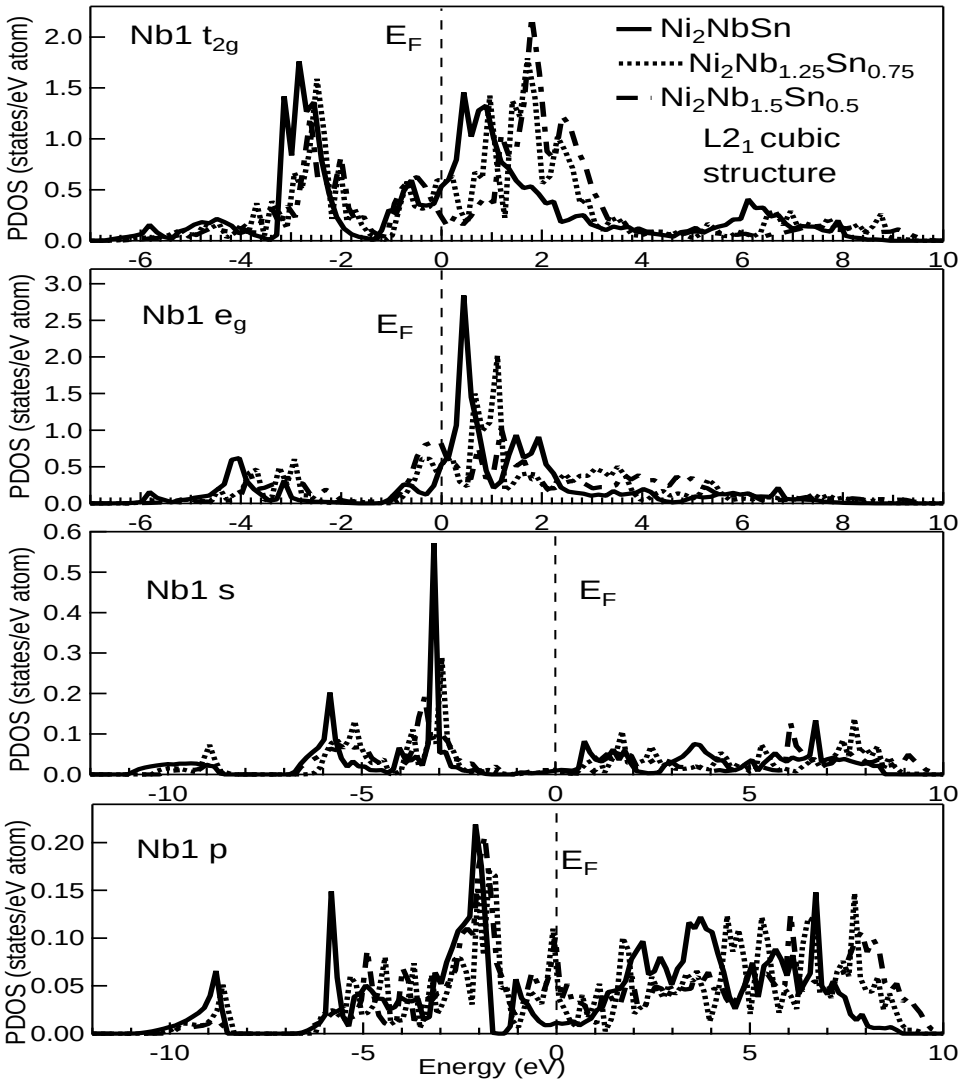

Figure 6: Spin integrated Nb1 PDOS of $Ni_2Nb_{1+x}Sn_{1-x}$ for $x = 0$, 0.25 and 0.5 in cubic $L2_1$ structure.

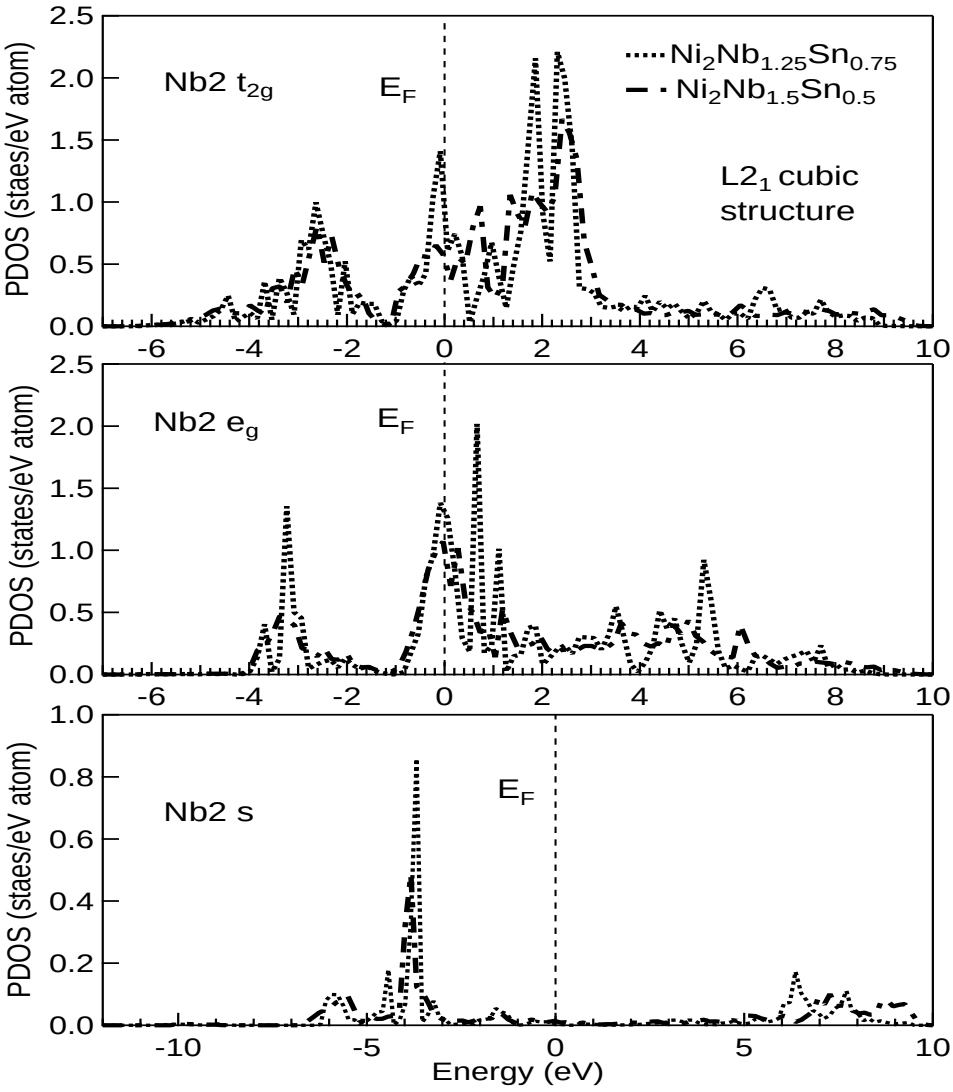

Figure 7: Spin integrated Nb2 PDOS of $Ni_2Nb_{1+x}Sn_{1-x}$ for $x = 0$, 0.25 and 0.5 in cubic $L2_1$ structure.

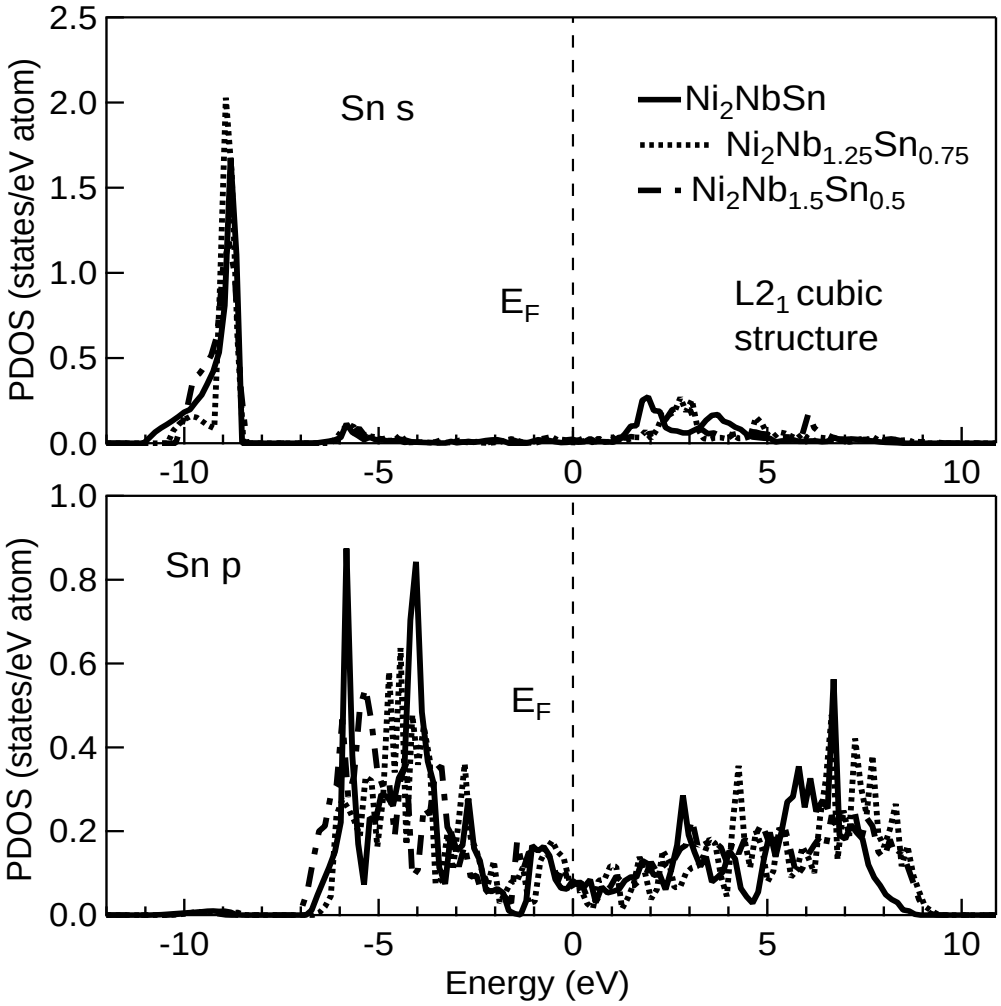

Figure 8: Spin integrated Sn PDOS of $Ni_2Nb_{1+x}Sn_{1-x}$ for $x = 0$, 0.25 and 0.5 in cubic $L2_1$ structure.

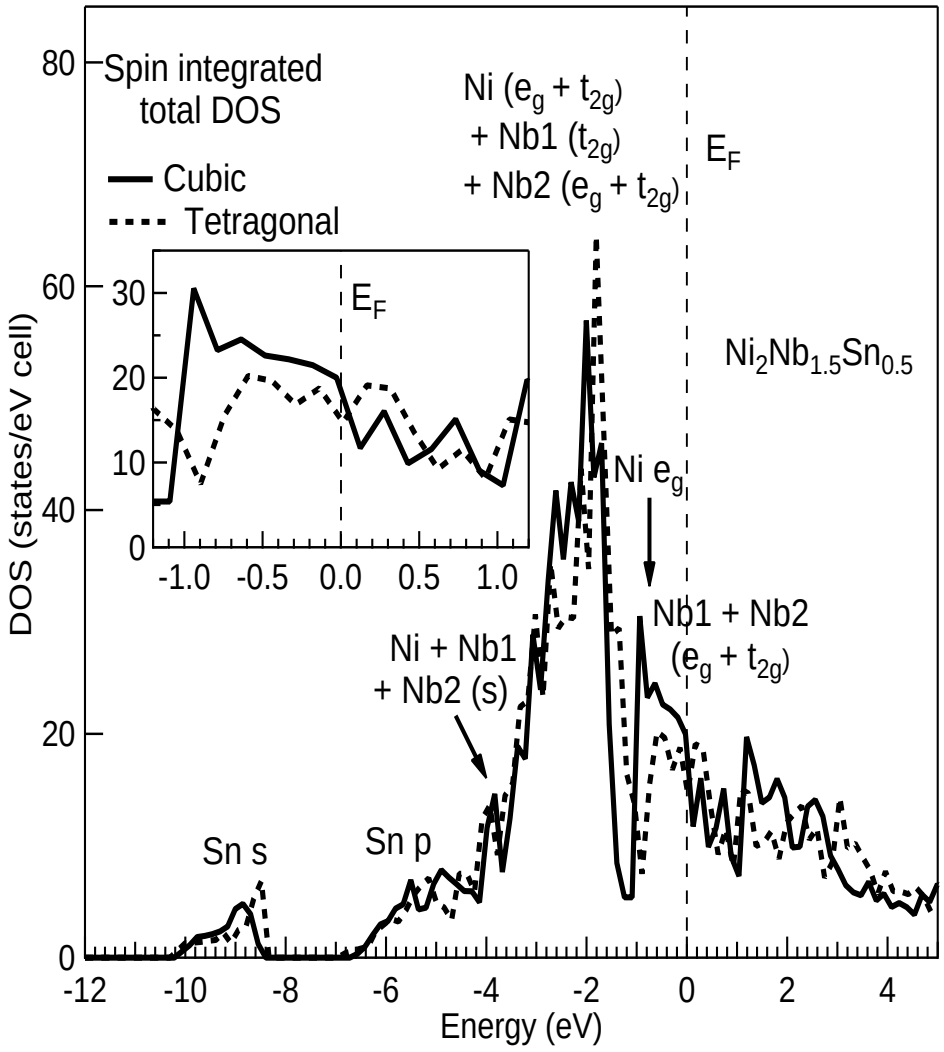

Figure 9: Spin integrated total DOS plot of $Ni_2Nb_{1.5}Sn_{0.5}$ in cubic $L2_1$ and tetragonal structures.

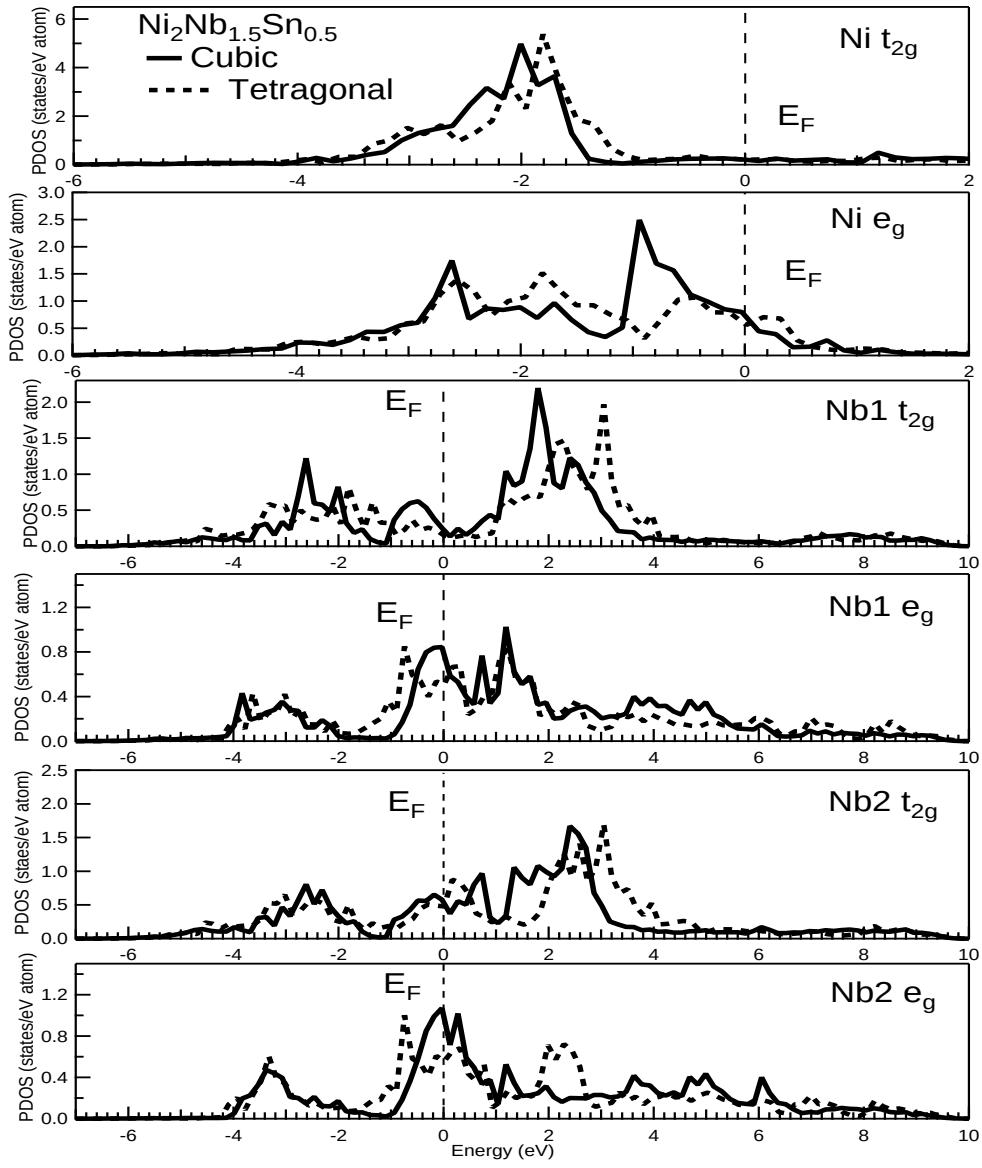

Figure 10: Spin integrated Ni, Nb1 and Nb2 3d PDOS plot of $Ni_2Nb_{1.5}Sn_{0.5}$ in cubic $L2_1$ and tetragonal structures.